Beam dynamics experiments to study the suppression of transverse instabilities

T. Houck
LLNL, Livermore, California 94550

S. Lidia
LBNL, Berkeley, California 94720

(Received 21 October 2002; published 5 March 2003)

Two-beam accelerators based upon relativistic klystron's (RK's) have been proposed as power sources for future generation linear electron-positron colliders. These drivers are susceptible to several transverse beam breakup (BBU) instabilities. An experiment to study a particular technique (the ''betatron node scheme'') for ameliorating the high-frequency BBU has been performed at LBNL on a 1 MeV, 500 A induction accelerator beam. The results of this experiment are particularly important for RK, but apply to any system where the betatron phase advance between perturbing structures is an integral multiple of 180°. This phase advance is beneficial in linear accelerators as the instability growth changes from exponential to linear. In the experiment described below, the beam is contained in a solenoidal focusing channel, rf cavities are spaced every 60 cm, and growth in the transverse motion was measured as a function of phase advance. Details of the experiment and results are presented.

DOI: 10.1103/PhysRevSTAB.6.030101 PACS numbers: 29.17.+w, 29.27.–a, 41.75.–i

I. INTRODUCTION

The relativistic klystron (RK) is a rf power source based on induction accelerator technology and conventional resonant output structures. Capable of generating hundreds of MW/m at frequencies up to *K* band, the RK has been proposed as a driver for a future linear collider in one version of a two-beam accelerator (TBA) [1]. A critical feasibility issue is the suppression of the transverse instability of the drive beam. This kiloampere beam must transit about a hundred resonance output structures and many hundreds of induction accelerator cavities if the RK is to achieve competitive efficiency and cost with respect to other proposed power sources. The RK's strong focusing used to contain the beam in the small aperture resonant structures, repetitive geometry, and reacceleration allows the resonant output structures to be spaced at a betatron phase advance of 360°. Significant theoretical studies and experiments have been accomplished in support of the relativistic klystron two-beam accelerator concept since it was initially described by Sessler and Yu in 1987 [2,3]. The relativistic klystron two-beam accelerator (RTA) program was established at LBNL in 1996 to study engineering and physics issues related to the construction of RK's suitable as rf power sources for TBA applications. A 1 MV, 1 kA induction injector, ancillary systems, and experimental hall were constructed. During the past year, we have performed beam dynamics experiments with the 1 MeV, 500 A beam produced by the injector. The experiment described below studied a technique for suppressing the growth of the transverse instability for the beam line geometry of an RK. Specifically, we have demonstrated a reduction of cumulative beam breakup (BBU) amplitude growth by more than 13 e-folds over a 10-period beam line with a technique for suppressing transverse beam instabilities that we refer to as the ''betatron node scheme.''

The outline of the paper is as follows. Section II describes the betatron node scheme (BNS). The experiment layout and major components are described in Sec. III. Details of the rf component designs used are given in Sec. IV. Measured values of the cavity parameters and the beam position monitor (BPM) response functions are given in Sec. IV. Two different modes of operation and data acquisition are described in Sec. V, along with a discussion of the experimental results. Observations and conclusions are then drawn in Sec. VI.

II. BETATRON NODE SCHEME

The BNS is based on the plausible scenario that a transverse kick given to a particle passing through a cavity will not result in a change in transverse offset at a cavity located an integer number of half-betatron wavelengths later. Without an increase in offset, the mechanism for exponential growth of the transverse instability is avoided. This effect can be seen implicitly in the theoretical derivation of [4]. In this reference, the motion of the beam centroid in a rotating coordinate system is treated with transfer matrices. For a linear system of thin cavities, the radial displacement and momentum of the centroid, r and p_r, entering a cavity can be related to the r and p_r entering the previous cavity by a combination of two matrices:

$$\begin{pmatrix} r \\ p_r \end{pmatrix}_n = \begin{pmatrix} \cos(\theta) & \frac{1}{\omega}\sin(\theta) \\ -\omega\sin(\theta) & \cos(\theta) \end{pmatrix} \begin{pmatrix} 1 & 0 \\ R & 1 \end{pmatrix} \begin{pmatrix} r \\ p_r \end{pmatrix}_{n-1}, \quad (1)$$

where θ is the betatron phase advance and ω is the betatron frequency. R is an integral operator that

 1098-4402/03/6(3)/030101(9)$20.00

describes the interaction of the beam with the cavity and is expressed as

$$Rr_n = \frac{e\omega^2 Z_\perp}{c^2 Q}\int e^{-[\omega(t-t')/(2Q)]} I(t') r_n(t') \sin\omega(t-t')dt', \tag{2}$$

where $Z_\perp$ is the transverse impedance, I is the beam current, and Q is the cavity quality factor. The first matrix describes the betatron oscillation of the beam between cavities. The second matrix describes the transverse impulse the beam receives as it passes through a cavity. The motion of the beam centroid at any location can be determined by repeated matrix multiplications.

The multiplication is straightforward, but difficult to perform analytically. However, in the case of small θ, it was shown in [4] that the solution reduces to the exponential growth from the standard continuum model [5]. For the special case where the phase advance between cavities is maintained at an integer multiple of π, the multiplication becomes trivial and

$$\begin{pmatrix} r \\ p_r \end{pmatrix}_n = \begin{pmatrix} 1 & 0 \\ R & 1 \end{pmatrix}^n \begin{pmatrix} r \\ p_r \end{pmatrix}_1 = \begin{pmatrix} 1 & 0 \\ nR & 1 \end{pmatrix} \begin{pmatrix} r \\ p_r \end{pmatrix}_1. \tag{3}$$

The authors of [4] recognized the significance of the linear growth indicated in Eq. (3) and suggested designing a linear induction accelerator based on this principle. However, there were practical issues related to the required strong focusing and energy flatness, and the concept was not pursued.

A group at the University of Michigan rediscovered the suppression of the instability for cavity spacing equal to the integral number of half-betatron wavelengths [6]. They derived the dispersion relations for a system of discrete cavities where the betatron wavelength did not greatly exceed the spacing of the cavities, i.e., where the continuum model was not applicable. Their dispersion relationship is expressed as

$$\cos\left(\frac{L\Omega}{v}\right) = \cos\left(\frac{L\omega_c}{v}\right) + \frac{\Gamma L}{2\omega_c v}\sin\left(\frac{L\omega_c}{v}\right), \tag{4}$$

where L is the cavity spacing, ω_c is the cyclotron frequency, v is the electron velocity, and $\Omega = \omega - kv$. The coupling of the beam to the cavity is included in Γ:

$$\Gamma = \frac{2\omega_o^4 \varepsilon}{\omega_o^2 - \omega^2 + i\omega\omega_o/Q}, \qquad \varepsilon = \frac{c}{60\omega_o L}\frac{Z_\perp}{Q}\frac{I}{17}\frac{\beta}{\gamma}. \tag{5}$$

I is the beam current in kA and ω_o is the cavity mode frequency. Equations (4) and (5) were used to calculate the expected growth of a cavity's peak dipole power due to the transverse motion of the beam as a function of phase advance between cavities. We calculate the dispersion relation using the BNS experiment (described below) design parameters. The beam energy was 1 MeV, the current was 600 A, $Z_\perp/Q = 13\ \Omega$, cavity dipole frequency = 3.75 GHz, and the cavity spacing was 60 cm for the calculation. Results are shown in Fig. 1. Power is for the tenth cavity normalized with respect to the first. The calculation assumes the pulse length is sufficiently long for the power to reach a maximum. The design cavity Q was 120, but to be comparable to the simulation shown in Fig. 2, it is necessary to account for the de-Q-ing effect of the energy spread from space charge depression. This energy spread is similar to an external Q of about 55.6 due to the spread in betatron frequencies resulting in a total Q of 38.

The concept was again rediscovered in simulations during a design study of an RK-TBA where the cavities were fortuitously spaced at $\lambda_\beta/2$ [3,7]. The main power extraction section of an RK uses strong focusing to transport the beam through small aperture rf output cavities and the beam energy is cyclic with respect to the cavities. This leads to a large and constant betatron phase advance between cavities.

Unlike the prior "discoveries," a specific accelerator design was being considered that was amenable to this technique. This encouraged further simulations to study the effects of cavity length, errors in phase advance, and beam energy or focusing variations. The importance of the BNS technique to the viability of efficient relativistic klystrons eventually justified an experimental study in the parameter range of operational interest.

Figure 2 is a simulation used in the design of our BNS experiment described below. A beam energy of 1 MeV with a 2% energy spread due to space charge depression, current of 600 A, and a 50 ns rise time followed by a 150 ns flattop was used for the simulation. The simulation calculated the transverse motion on the beam for a single dipole mode trapped in cavities spaced every 60 cm with $Z_\perp/Q = 13\ \Omega$, $Q = 120$, and frequency = 3.75 GHz. The simulated beam was given an initial transverse "seed," $x(z = 0, t) = \sin(\omega_o t)$, to represent the frequency component of the noise signal at the dipole resonance. The peak power during a time window of 70 to 200 ns

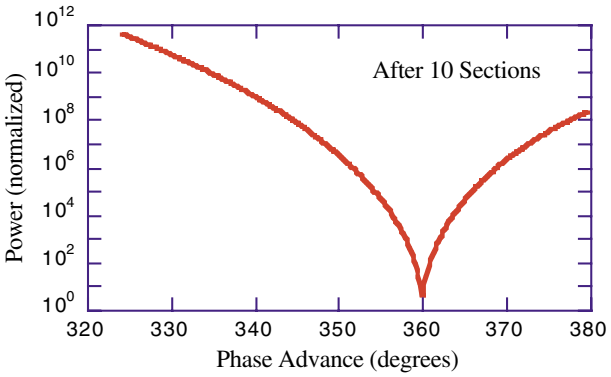

FIG. 1. (Color) Cavity dipole mode power as a function of phase advance.

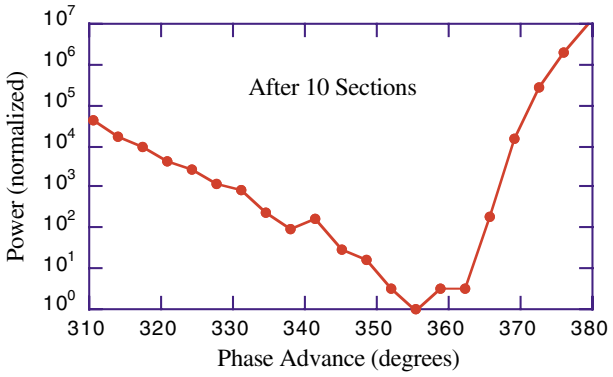

FIG. 2. (Color) Simulation of expected growth for the transverse instability in the BNS experiment.

after the beam exited the tenth cavity is plotted in Fig. 2 as a function of betatron phase advance between cavities. Power is for the tenth cavity normalized by the seed power.

There is good agreement between the growth predicted by Eq. (5) shown in Fig. 1 and the simulation results shown in Fig. 2 when the phase advance is larger than 360°. The growth of the instability as a function of time during the beam pulse is shown in Fig. 3 for a phase advance of about 370° per cavity. The growth reaches a constant value within 70 ns after the initial rise time.

However, for the underfocused case, i.e., phase advances less than 360°, the dispersion relationship produces substantially different results than the simulation. The temporal behavior of the growth for the underfocused case is much more complex as illustrated in Fig. 4. The variation in growth well after the head of the beam qualitatively indicates interference between the betatron motion of the beam and the excitation of the regularly spaced cavities that is slowing the instability growth. The lower than expected growth for the underfocused case results in a noticeable asymmetry in growth about a phase

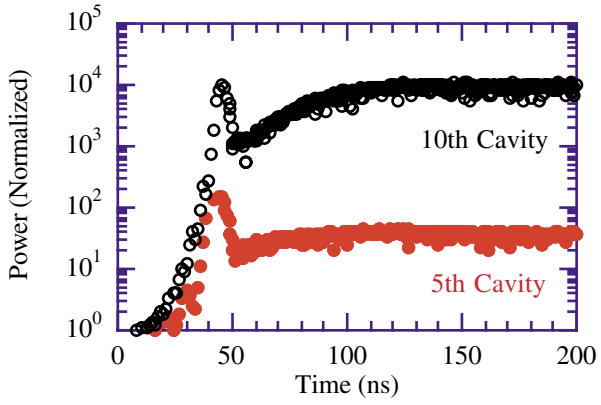

FIG. 3. (Color) Simulation of expected growth of the transverse instability as a function of time during the beam pulse for two different cavities. Phase advance per cavity = 370°.

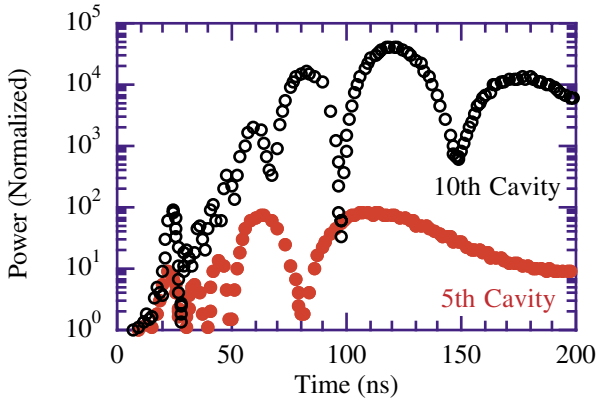

FIG. 4. (Color) Simulation of expected growth of the transverse instability as a function of time during the beam pulse for two different cavities. Phase advance per cavity = 310°.

advance of 360° relations. This asymmetry in growth has been noted by the authors in simulations for a wide variety of accelerator parameters including full scale RK's [3].

It is important to point out that the above simulations were performed for a single mode. This is not a significant limitation, however. For phase advances not near an integer multiple of 180°, the exponential growth factor is proportional to

$$\Gamma \propto \omega_o \left(\frac{Z_\perp}{Q}\right) Q_{\text{Total}}, \tag{6}$$

where ω_o is the frequency, $Z_\perp/Q$ is the shunt impedance, and Q_{Total} is the total Q for the mode. The mode with the largest growth factor will dominate the motion of the beam due to the exponential growth. However, Eq. (3) indicates that the growth in displacement due to all transverse modes will be changed from exponential to linear as the betatron phase advance approaches an integer multiple of 180°.

This fact proved to be very beneficial, but also a slight hindrance in the actual experiment. The simulations were used primarily for the experiment design to ensure that the growth with phase advance about 360° was not too great for the expected resolution of the experiment, i.e., the v shape of Figs. 1 and 2 was not so sharp that we would not be able to adjust the focusing of the transport solenoids without missing the minimum. There were some limitations on ω_o and Q_{Total} that will be described below, but as long as the product of the three components in Eq. (6) remained relatively constant, the steady-state simulation results would be the same. Because of low quality material used to load the rf cavities, the individual cavity dipole frequencies varied greatly (refer to Table I) and there was concern that the growth factor would be insufficient. Fortunately, in operation an unanticipated transverse mode of higher frequency (5.36 GHz) and lower impedance, but acceptable growth, was discovered

TABLE I. Pillbox cavity dipole mode parameters.

Cavity	Frequency (GHz)	Q
1	3.76	100
2	3.794	120
3	3.754	110
4	3.925	140
5	3.85	110
6	3.99	120
7	3.715	130
8	3.377	150
9	3.5	100

that permitted the successful measurement of BNS mode suppression.

Measurements of the growth of the transverse motion are more difficult as the phase advance approaches an integer multiple of 180° as the relative growth of different modes is not nearly as pronounced. As in our case where the growth is starting from noise, it can take a number of cavities (periods) before a particular mode dominates other transverse modes that may have started from a larger noise component.

III. DESCRIPTION OF BNS EXPERIMENT

The experiment measures growth in the high-frequency transverse oscillation of a 250 ns (FWHM), 500 A, 1 MeV electron beam. This cumulative BBU mode is common in all linear accelerators and beam lines with trapped dipole modes in periodically spaced rf structures. The experimental hall with the injector and beam line is shown in Fig. 5. The pulsed power units and power supplies for the solenoids are housed in the racks to the right of the injector.

A. Injector

The injector has been described elsewhere [8]. It uses a diode arrangement with a 3.5 in. diameter, dispenser

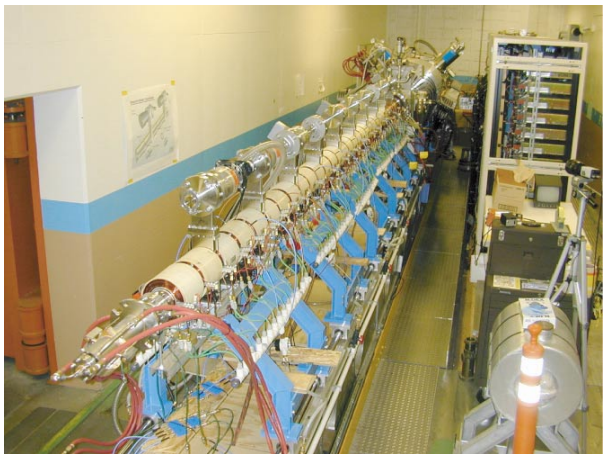

FIG. 5. (Color) Photograph of the RTA experimental hall.

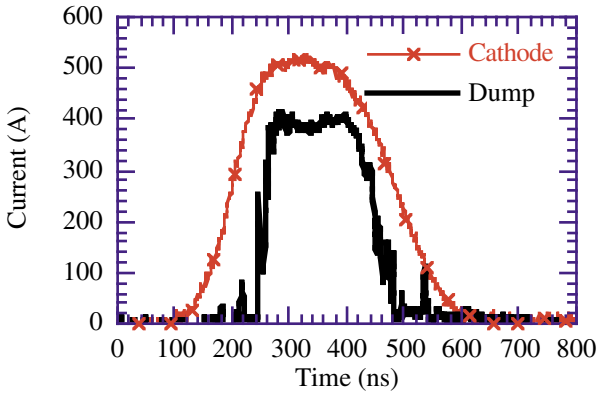

FIG. 6. (Color) Typical cathode and dump current pulses.

cathode and has a perveance of about 0.58 μperv. The 24 induction cells are divided evenly between the anode and cathode halves of the injector and provide about 42 kV per cell.

Beam energy was determined by summing the voltage at each cell. Capacitive probes were also used to measure the voltage and pulse shape for both cathode and anode stalks. Representative current pulses from the cathode and dump current monitors are shown in Fig. 6. The transition section of the beam line prior to the BNS section acts as an energy selector, effectively scraping off the leading and trailing edges of the pulse. For the pulses shown, the average beam energy was approximately 930 kV $\pm$ 3% with a relative variation of $\pm$1.4% during the 130 ns of "flattop."

B. BNS section

The 6 m of the beam line involved in the experiment is composed of a set of 10 periods. A period is made up of one rf pillbox cavity, one capacitive button BPM, one vacuum pumping port, three nipple flanges for vacuum containment, and three fine wire solenoids for beam focusing and transport. A schematic of a two-period length is shown in Fig. 7. The ~60 cm spacing is about a λ_β for a nominal 1 MeV beam and an average axial

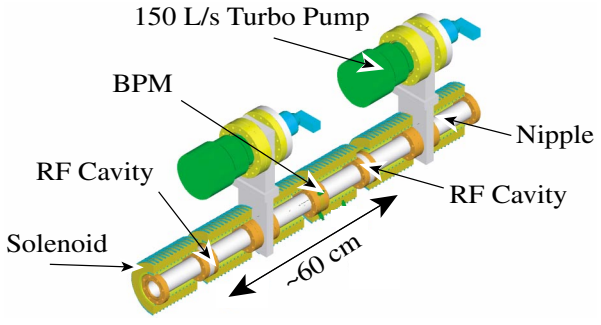

FIG. 7. (Color) Repeating beam line section in BNS experiment.

magnetic field of around 1 kG. The successful demonstration of the technique used to damp the BBU growth relied upon the modular design of the beam line, precise tuning of the transport magnets, and careful design of the beam position monitors. These components will be described in detail below.

IV. RF COMPONENT DESCRIPTIONS

The choice of the dipole mode frequency excited within the cavities, and detected at the BPMs, was made by balancing the requirements of high frequency with high beam transmission. The high-frequency requirement ensured that the rf period was much less than the beam pulse rise time or flattop, and that steady-state conditions would be achieved. A higher frequency requires a smaller beam line aperture such that the cutoff frequency remains above the mode frequency. Transmission of the beam pulse through the system using reasonable solenoid fields and for a variation of a least $\pm 10\%$ in field value (phase advance) was a necessity and leads to larger apertures. Off-the-shelf components for the beam line were chosen whenever possible to help decrease the overall cost of the experiment. A relatively short betatron wavelength was required so that multiple betatron oscillations could be obtained with a fairly short (<10 m) transport line. The multiple oscillations were important in the event that the growth factor was smaller than anticipated or separation of competing modes was needed.

We chose standard MDC 2 in. OD (outer diameter) nipples with 3 and 3/8 in. conflat flanges as the basic building blocks of the system. This allowed for a 1.87 in. ID (inner diameter) aperture for beam transport between cavities and BPM's. Each 6.45 in. long nipple supports a fine wire solenoid with 87×14 turns. 1 kW or 3 kW power supplies (Sorenson's DCS50-20 and DCS150-20) provided up to 16 A of current to either individual solenoids or solenoid triplets. Fields of up to 1.5 kG could be easily produced. To minimize magnetic field holes, pumping ports were constructed from MDC GV-2000M gate valve bodies, equipped with multi-Lam finger stock tack welded onto the ID to provide a current-return path. Three nipples are used to form the periodic unit cell of the beam line. Between each nipple is an MDC double-sided, 3 and 3/8 in. OD conflat flange that holds an rf cavity, a BPM, or a pumping port.

A. Dipole pillbox cavities

Physics, construction, and assembly requirements dictated that single flange widths only be used between nipples, and that the solenoids were able to slide over the rf cavities. The OD of the pillbox cavity volume is limited to the 2 in. ID of the conflat flange. This dictated the use of dielectrics to load the cavities and lower the dipole mode frequencies so that the modes would be trapped. Additional stainless steel pipe sections were brazed and tack welded onto the flange to hold the dielectric ring insert, as well as to provide an additional cutoff region for the mode.

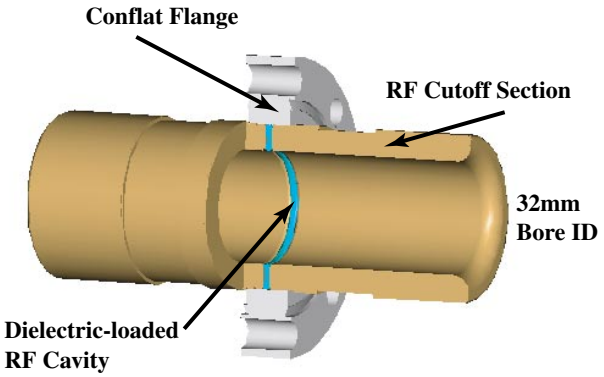

FIG. 8. (Color) Schematic of dipole mode pillbox cavity.

We chose to use 96% alumina as the dielectric material. The cavity gap itself is 2 mm wide, with a 26 mm outer radius, and a 16 mm inner radius defined by the cutoff pipe ID. The alumina insert has a 26 mm outer radius and a 8 mm radial thickness. This produces a dipole TM_{110} mode with frequency ~ 3.75 GHz. A schematic of the rf cavity is shown in Fig. 8.

B. Capacitive button beam position monitors

The capacitive button BPMs copied the same basic construction as the rf cavities. They are built from single conflat flanges, with a brazed stainless steel cutoff section that acts as a high-pass filter. The BPMs themselves are standard button-type. The BPM button electrode is made of 0.125 in. OD OFHC copper stock, and inserted within a 0.3 in. ID bore hole. This bore hole penetrates from the outer surface of the flange through the inner surface of the brazed-on stainless steel pipe insert. A 50 Ω coaxial SMA vacuum feedthrough is welded onto the outer surface of the flange. From there, individual button signals

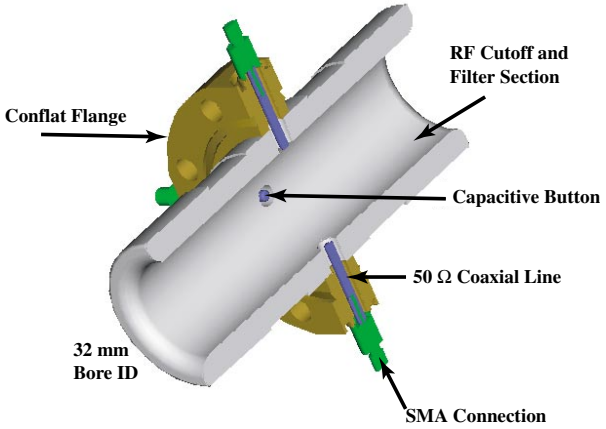

FIG. 9. (Color) Schematic of capacitive BPM.

are collected and either sent directly to the data acquisition oscilloscopes, or are combined with a set of 2–4 GHz, 180° 3-dB microwave hybrids (Anaren 30056) which then transmit Δx, Δy, and sum signals after rectification with microwave detectors (Agilent 8474C). A schematic of the BPM is shown in Fig. 9. The −3 dB knee in the button response transfer function is located at ~1.2 GHz. With a 50 Ω load and 2.6 pF button shunt capacitance, the RC time constant is ~0.13 ns.

C. Cavity mode parameters

The electromagnetic simulation and design code GDFIDL [9] was used to design the rf cavities. For a 2 mm long gap, and with dielectric loading, GDFIDL predicts a dipole, TM_{110} mode with frequency ~3.75 GHz. The normalized, transverse shunt impedance, $[Z_t/Q] = [R/Q]/(k^2x^2)$, is then given to be ~13 Ω.

A microwave vector network analyzer (HP 8510) was used to measure the dipole mode frequency and Q values. A 100 Ω, two-wire transmission line was used to measure the monopole and dipole scattering parameters from 2–4 GHz [10]. From the S_{12} parameters were measured the cavity frequencies and Q values. The measured values of the ten cavities used in the beam line are listed in Table I.

The unexpected spread in dipole mode frequency between the different cavities is thought to originate from poor quality control over the grade of alumina used for the dielectric rings. A higher grade of alumina was procured, but the experiment was completed before replacement cavities could be fabricated.

D. BPM response function

The transfer impedance of the individual BPM buttons was measured using the same microwave test stand as for the cavities [10]. The individual responses were combined in software to calculate the overall BPM response to transverse beam oscillation in the 2–4 GHz range. The response function is shown in Fig. 10.

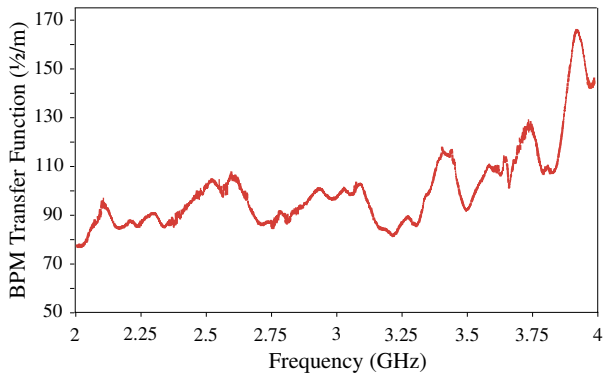

FIG. 10. (Color) Response function of a BPM.

E. General comments on rf components

In retrospect, it would have been wise to invest in rf components that covered a greater frequency band than the 2–4 GHz chosen. The rf cutoff and filter section had a cutoff frequency of 5.5 GHz and confined the planned 3.7 GHz dipole mode. The section was not sufficiently long to adequately trap modes above 4 GHz and initial simulations did not indicate any transverse modes above 4 GHz with non-negligible impedance. The BPM response function was not evaluated above this value since the initial plan was to filter out all higher frequency components. The BPM design was reasonably broadband and adequate for frequencies up to about 10 GHz. The power spectrum measurements described below were relative measurements and did not use the response function.

V. MEASUREMENTS

Two different modes of data acquisition were employed during beam operations. The first looked at the rectified signals integrated over the 2–4 GHz microwave hybrid bandpass spectrum. The second looked at the raw BPM signal, mixed down in frequency with a local oscillator (HP 8690B) and monitored with a frequency counter (HP 5351B), then captured on a fast oscilloscope (Tektronix TDS654).

In the first mode, no definite signals were observed in the expected 2–4 GHz range. This is thought to be due to the small amount of gain of the instability from the lack of overlap between the dipole modes of the different cavities.

The second mode of measurement displayed a strong signal at approximately 5.35 GHz. We believe that the 5.35 GHz mode is related to the geometry of the beam line and not the rf cavity. There was no externally driven cavity. The transverse instability was excited by noise and offsetting the beam from the axis with dipole steering coils. This resulted in the excitation of all modes associated with the cavities and beam line. However, the modes

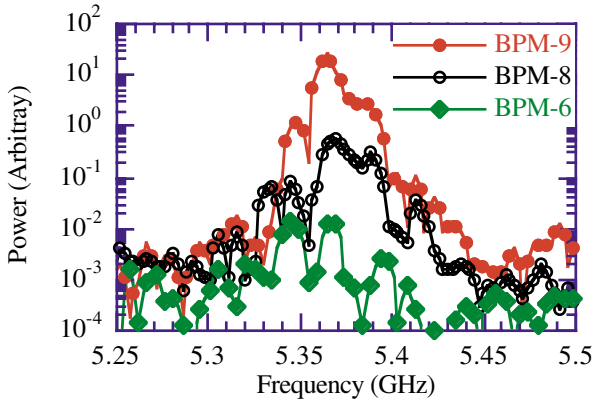

FIG. 11. (Color) FFT power spectrum for 6th, 8th, and 9th BPM's.

with the highest impedance dominated the spectrum after a few sections of the beam line. As shown in Fig. 11, the transverse dipole instability grew rapidly at this frequency as measured from BPM to BPM along the beam line. The data for Fig. 11 were taken at a phase advance of 344°.

A. Growth as function of focusing

Figure 12 shows the growth in the power of the 5.36 GHz transverse mode from BPM 7 to BPM 9 as a function of betatron phase advance between rf cavities. The error bars in phase relate to the ±1.4% variation in energy during the flattop portion of the pulse. Note that a 6° change in phase is equivalent to about a 1.5% change in magnetic field or beam energy. The mode power grew from noise so it was necessary to reference the power at a BPM to that at an earlier BPM to correct for variations in the noise signal. For phase advances of less than ~340° the 5.36 GHz component of a BPM's fast-Fourier transform (FFT) power spectrum could be reliably separated from competing modes by the fifth BPM. Near 360° of phase advance, it was difficult identifying the mode until at least the sixth BPM and we chose to use the seventh as the reference. The opposite difficulty occurred with BPM 10. The magnitude of the transverse beam motion was sufficient to cause some beam loss, particularly noticeable for phase advances above 360°, resulting in an unreliable signal. BPM 9 did not exhibit this problem until the phase advance was increased above ~370° or below ~335°.

The total growth from the initial cavity to the eighth cavity (prior to BPM 9) can be estimated by raising the power shown in Fig. 12 to the fourth power. The exponential growth is proportional to the number of cavities. At the extreme limits of the scan this would equate to a power growth of almost 12 orders of magnitude greater than for the minimum, or 13 e-foldings of the transverse beam motion.

For this data the beam energy was held constant and the solenoid current varied. The asymmetric growth of power about 360° phase advance is a characteristic feature of the betatron node scheme observed in simulations for several different configurations [3].

The 5.36 GHz frequency mode excited in the experiments was not anticipated to be the prevalent transverse mode. The Q of the mode can be estimated from the frequency spectrum; see Fig. 11. The half power bandwidth of this mode was very close to, if not limited by, the spectrum frequency resolution of 50 MHz. Thus $Q \geq 110$. The exponential growth factor is given by

$$\Gamma = \frac{\omega_o Z_\perp}{30cl}\frac{I}{17}\int_0^L \frac{dz}{\gamma_\beta} \geq 13, \tag{7}$$

where l is the cavity spacing (0.6 m), I is the current in kA (0.4), L is the length of the beam line in meters, and 13 is the estimated number of e-foldings for the nine periods. For our experiment, $Z_\perp \geq 482\ \Omega$ and $Z_\perp/Q \geq 4.4\ \Omega$. This is a low estimate as the peak growth should not have been reached for the range of phase advance used.

B. Growth along the beam line

Figure 13 shows the increase in growth as the signal is measured along the beam line for an underfocused condition and a nominally on-focus condition. Only the last four periods are shown with BPM 6 used as a normalizing value. For earlier periods the relative low signal strength and number of modes with comparable power levels made consistent measurements problematic. Eight signals, both an x and y orientation for each BPM, were recorded during a single pulse for Fig. 13. Two sets of measurements are shown for each phase advance to indicate the pulse-to-pulse variation in relative growth. An underfocused deviation of 18° from the desired 360° of betatron phase advance between cavities clearly shows the expected exponential growth. Within experimental uncertainty, the theoretical linear growth is realized as the phase advance approaches 360°.

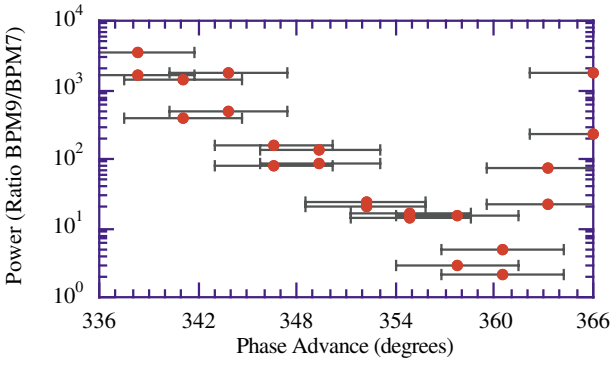

FIG. 12. (Color) Spectral peak power as a function of phase advance.

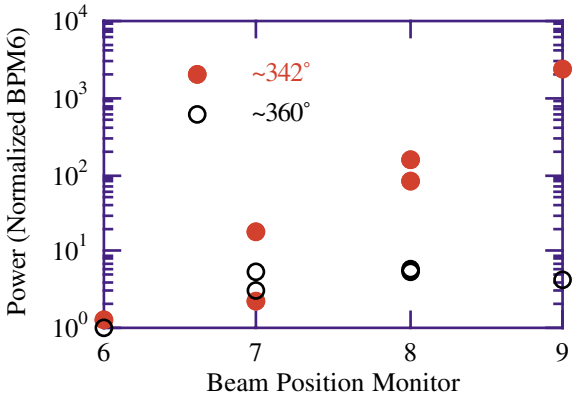

FIG. 13. (Color) Spectral peak power as a function of BPM position for two different betatron phase advances.

C. Determining beam energy

The BNS experiment actually is a beam energy analyzer. The solenoidal focusing field and cavity spacing are known to a few tenths of a percent. The solenoid current that yielded the minimum growth for the data shown in Fig. 12 was assumed to produce a betatron wavelength equal to cavity spacing. We then calculated that the required beam energy was approximately 955 KeV $\pm$ 0.5% due to uncertainty in determining the minimum. The 955 KeV value falls within the range of energy from summing individual induction cell voltages and the accuracy is significantly improved.

A feedback system could easily be constructed around BPM's, or other diagnostics, capable of monitoring power in transverse modes. The betatron phase advance would then be adjusted to minimize the power by varying either the beam energy and/or focusing strength of the transport magnets.

VI. CONCLUSIONS

We had expended considerable effort in the design and fabrication of the rf components for the BNS experiment, and the unexpected variation in cavity resonant frequency from the expected 3.75 GHz was disappointing. Time constraints dictated that we proceed with the experiment while waiting for new materials even though the strength of the instability was going to be substantially lower than initially planned. The instability at 5.36 GHz was unexpected, but proved to be fortuitous allowing the BNS damping scheme to be observed.

The modular design of the experiment ensured that any undamped resonances would be sources for beam instabilities. The 5.36 GHz resonance was missed during the initial design because both simulations and microwave testing were performed on individual components. Once the 5.36 GHz instability was observed, a full period (60 cm length) mockup of the BNS beam line was placed on the microwave test stand. A dipole mode was then observed at $\sim$5.30 GHz with the 2-wire transmission line. GDFIDL simulations of a full beam line period showed a high longitudinal order, $\sim$5.24 GHz transverse mode in the beam pipe region between the rf cavity and the BPM that included the pumping port. The desire to use identical parts for ease of construction and operation meant that we kept the longitudinal spacing identical for a constant phase advance. Each period of the BNS beam line can then be considered an extended cavity with the original rf cavity as a negligible perturbation.

The longitudinally extended character of the transverse mode presents a challenge to our simulations. In principle, the BNS technique should work on any independently driven, localized transverse mode that is periodically distributed. However, the theoretical analysis presented in Sec. II implicitly assumed that the transverse kick to the beam occurs at discrete locations. The simulation code used in the design of the experiment allows for a finite cavity width, but requires the kick to occur over a small fraction of the betatron wavelength. A full electromagnetic, particle code would be required to accurately simulate the problem, and it would need to be able to track the particles through several betatron wavelengths.

An argument often made against the BNS scheme is that it may work under the ideal conditions assumed in theoretical derivations, but for practical systems the inherent energy variations and system tolerances will hide the effect. Simulations have tried to model practical situations, but normally with some assumptions required. However, it has now been shown under very average conditions that the BNS effect is real. For the data shown, there was a 50 ns rise time to the current pulse, the beam energy varied $\pm$1.4% over the flattop portion of the pulse, and no special alignment or machining tolerances were used in the fabrication and assembly of the experiment. In fact, an unplanned instability source was damped. Also, only standard diagnostics are required to determine the optimum focusing field. It will be interesting to see if future accelerators or klystrons will incorporate this scheme.

ACKNOWLEDGMENTS

We thank our Technical Steering Committee, Yu-Jiuan Chen, Roberto Cosini, Rainer Pitthan, Andy Sessler, Glen Westenskow, and Simon Yu, for their guidance and advice. Dave Vanecek supplied mechanical engineering and design support. Will Waldron was our pulsed power engineering. Stefano De Santis did the rf measurements and calibrations for the cavities and BPM's. The lead technicians were Wayne Greenway (mechanical) and Edgardo Romero (electrical). Carmen Frias assisted in the operation of the experiment during her Summer Internship. Management oversight and program support was provided by Bill Barletta, George Caporaso, and Kem Robinson.

[1] A. M. Sessler and S. S. Yu, Phys. Rev. Lett. **58**, 2439 (1987).
[2] G. Westenskow and T. Houck, IEEE Trans. Plasma Sci. **22**, 750 (1994).
[3] S. Yu, F. Deadrick, N. Goffeney, E. Henestroza, T. Houck, H. Li, C. Peters, L. Reginato, A. Sessler, D. Vanecek, and G. Westenskow, University of California, LBNL Report No. LBID-2085/UCRL-ID-119906, 1995.
[4] V. K. Neil, L. S. Hall, and R. K. Cooper, Part. Accel. **9**, 213 (1979).
[5] W. K. H. Panofsky and M. Bander, Rev. Sci. Instrum. **39**, (1968).
[6] R. A. Bosch, P. R. Menge, and R. M. Gilgenbach, J. Appl. Phys. **71**, 3091 (1992).

[7] H. Li, T. L. Houck, S. S. Yu, and N. Geoffeney, in *Design Consideration of Relativistic Klystron Two-Beam Accelerator for Suppression of Beam Break-Up*, SPIE Proceedings Vol. 2154-10 (SPIE–International Society for Optical Engineering, Bellingham, WA, 1994).

[8] S. M. Lidia, S. Eylon, E. Henestroza, D. L. Vanecek, S. S. Yu, T. L. Houck, G. A. Westenskow, and D. E. Anderson, in *Proceedings of the 1999 Particle Accelerator Conference, New York City, NY* (IEEE, Piscataway, NJ, 1999), pp. 3390–3392.

[9] Information on GDFIDL can be found at http://www.fbdb.de.

[10] S. Lidia, S. De Santis, and T. Houck, in *Proceedings of the 2001 Particle Accelerator Conference (PAC2001), Chicago, IL* (IEEE, Piscataway, NJ, 2001).